FORMATION OF NANOMETER-SCALE CONTACTS TO VISCOELASTIC MATERIALS

Implications for MEMS

K.J. WAHL
Code 6170
Naval Research Laboratory
Washington, D.C. 20375-5342

W.N. UNERTL
Laboratory for Surface Science & Technology
University of Maine
Orono, ME 04469

Abstract

The making and breaking of nanometer-scale contacts is an essential operation in MEMS devices with moving parts. The behavior of contacts in this size range is not well understood, especially if viscoelastic materials are involved. This article describes shear modulation spectroscopy, a new scanning force microscope technique especially well suited for quantitative studies of nanometer-scale contacts to viscoelastic materials such as lubricants and some polymers. The technique is illustrated by measurements and analysis of contacts to poly(vinylethylene).

1 Introduction

The operation of MEMS devices with moving parts requires the making and breaking of contacts with typical dimensions of 10-100 nm and loads in the nanoNewton to milli-Newton range. In general, these contacts may be subjected to both normal and shear loading. They may, or may not, be lubricated and the lubricant film may be as thin as a single monolayer. Recent theoretical [1,2] and experimental studies [3] suggest that continuum theories of contact mechanics [4] should be applicable to MEMS size contacts. However, factors such as adhesion [2,5] and capillarity [6] contribute more significantly compared to macroscopic contacts. In addition, other important factors, such as microslip [7] and viscoelastic response [8], may be altered when the contacts have dimensions comparable to the microstructure or molecular dimensions. A major experimental difficulty in the study of small contacts is the accurate measurement of the contact area.

In this article, we describe shear modulation spectroscopy (SMS). SMS is implemented with a scanning force microscope and provides quantitative information about nanometer-scale contacts including changes during loading and unloading. Emphasis is on contacts to viscoelastic materials. We also discuss the application of contact mechanics models that include viscoelastic response. The article concludes with a few remarks about the implications for MEMS technology.

Report Documentation Page

Form Approved
OMB No. 0704-0188

Public reporting burden for the collection of information is estimated to average 1 hour per response, including the time for reviewing instructions, searching existing data sources, gathering and maintaining the data needed, and completing and reviewing the collection of information. Send comments regarding this burden estimate or any other aspect of this collection of information, including suggestions for reducing this burden, to Washington Headquarters Services, Directorate for Information Operations and Reports, 1215 Jefferson Davis Highway, Suite 1204, Arlington VA 22202-4302. Respondents should be aware that notwithstanding any other provision of law, no person shall be subject to a penalty for failing to comply with a collection of information if it does not display a currently valid OMB control number.

1. REPORT DATE	2. REPORT TYPE	3. DATES COVERED
2007		**00-00-2007 to 00-00-2007**

4. TITLE AND SUBTITLE	5a. CONTRACT NUMBER
Formation of Nanometer-Scale Contacts to Viscoelastic Materials	5b. GRANT NUMBER
	5c. PROGRAM ELEMENT NUMBER
6. AUTHOR(S)	5d. PROJECT NUMBER
	5e. TASK NUMBER
	5f. WORK UNIT NUMBER
7. PERFORMING ORGANIZATION NAME(S) AND ADDRESS(ES) **Naval Research Laboratory,Code 6170,4555 Overlook Avenue, SW,Washington,DC,20375**	8. PERFORMING ORGANIZATION REPORT NUMBER
9. SPONSORING/MONITORING AGENCY NAME(S) AND ADDRESS(ES)	10. SPONSOR/MONITOR'S ACRONYM(S)
	11. SPONSOR/MONITOR'S REPORT NUMBER(S)

12. DISTRIBUTION/AVAILABILITY STATEMENT
Approved for public release; distribution unlimited

13. SUPPLEMENTARY NOTES
The original document contains color images.

14. ABSTRACT

15. SUBJECT TERMS

16. SECURITY CLASSIFICATION OF:			17. LIMITATION OF ABSTRACT	18. NUMBER OF PAGES	19a. NAME OF RESPONSIBLE PERSON
a. REPORT	b. ABSTRACT	c. THIS PAGE			
unclassified	**unclassified**	**unclassified**		**11**	

2 Basics of Shear Modulation Spectroscopy

Shear modulation spectroscopy [7] is an extension of the well-developed mechanical modulation techniques used to measure the viscoelastic and rheological properties of bulk polymers [9] and has been used previously to study elastic behavior in scanning force microscope contacts [10-13]. Similar measurements on much larger area contacts have been made with the surface forces apparatus [14,15] and microscopic sphere-on-flat contacts [16]. SMS is also closely related to friction loop methods [17] and to force modulation spectroscopy [18,19].

Both SMS, which uses shear modulation, and force modulation spectroscopy, which modulates the contact normal to the surface, provide information about the viscoelastic properties of the contact. However, SMS has two significant advantages over force modulation spectroscopy. First, since the normal load is constant in SMS, the contact area does not change during a modulation cycle. This simplifies the analysis. Second, during normal modulation, the end of the cantilever moves up and down along a circular arc. Thus, the contacting tip always has a small component of shear motion parallel to the surface. As shown recently by Mazeran and Loubet [20], this combined normal and lateral motion significantly complicates quantitative interpretation of the force modulation spectroscopy data.

2.1 SHEAR MODULATION SPECTROSCOPY

Figure 1a illustrates how SMS is carried out with a scanning force microscope. The scanning force microscope tip (height H) is placed in contact with a viscoelastic sample above point O under applied load F_N. The substrate is then displaced parallel to its surface by distance x_o to O'. This causes a displacement of the tip's contact point by $x_t = x_o - x_c$ where x_c is the distortion of the sample surface relative to point O'. This distortion results from the shear force $F_s =$ x_t, where is the torsional stiffness of the cantilever. For a viscoelastic material and oscillatory sample displacement $x_o(t) = X_o$- exp(i t), the contact of the tip on the surface is displaced by $x_t = X_t$exp[i(t -)] which has a phase lag α. The experimentally measured quantities are the amplitude and phase of the tilt angle of the tip; $= x_t / H =$ $_o$exp[i(t -)] where $_o \equiv X_t/H$ and X_t is the amplitude of the tip motion at the contact. The shear stiffness of the contact is $_c \equiv dF_s/dx_c$. For the case of an elastic Hertzian contact with no slip, $_c = 8G^*a$ where a is the effective radius of the contact.

Figure 1b shows the relationships between the amplitudes and phases of the various motions. Starting from the condition $x_t = x_o - x_c$, the amplitude and phase of the contact displacement can be expressed in terms of the measurable quantities as

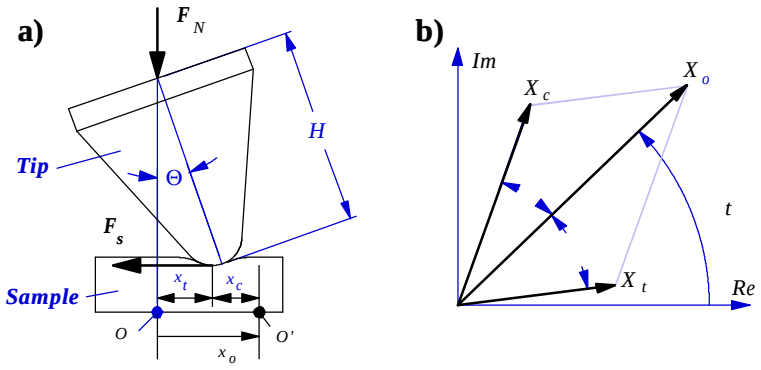

Figure 1. (a) Schematic diagram of the scanning force microscope shear measurement. (b) Relationship between the amplitudes and phases.

$$\frac{X_c}{X_o} = \sqrt{1 + \left(\frac{X_t}{X_o}\right)^2 - 2\left(\frac{X_t}{X_o}\right)\cos} \qquad (1)$$

and

$$\sin = \frac{\left(\frac{X_t}{X_o}\right)\sin}{\sqrt{1 + \left(\frac{X_t}{X_o}\right)^2 - 2\left(\frac{X_t}{X_o}\right)\cos}}. \qquad (2)$$

The phase angle is the more robust quantity. It requires only a relative measurement of the displacement amplitude of the tip whereas determination of X_c requires absolute knowledge of X_o, which is typically only a few tenths of a nanometer.

2.2 EXPERIMENTAL ASPECTS OF SMS

SMS can be implemented on any scanning force microscope capable of making quantitative measurements of the torsional and bending motions of the cantilever force detector. We used a scanning force microscope that has been described previously [21] and is based on the optical lever method. The sample is oscillated laterally with respect to the cantilever by applying a small sinusoidal modulation, typically ≈ 0.1-0.2 nm, to the piezoelectric scan tube. This amplitude is well below the value required to initiate sliding, except as the contact initially forms and just prior to release [7]. The photodiode detector output is analyzed with a lock-in amplifier to obtain the amplitude X_t and phase of the torsional response of the scanning force microscope cantilever. The amplitude of the shear force acting on the tip can be obtained from $|F_s| =$ X_t if the torsional force constant is known. For the cantilevers we used $\approx 67H$ where $H \approx 4$ μm is the tip height [22].

The poly(vinylethylene) (PVE) samples discussed below were made from the same 96% 1,2-polybutadiene material with 134,000 number-average molecular weight used in a previous study of the bulk mechanical properties [23]. From this study, the measured bulk relaxation time at 289 K is $_b \approx 60$ μs. Young's modulus was measured by indentation to be in the range 2-4 MPa. Films of PVE were cast onto glass slides from toluene solution, dried in air for about 10-15 min, followed by vacuum drying for another 10-20 min. Since the surface properties of the PVE samples were found to vary slowly for several days following preparation [7], only freshly prepared samples were used to obtain the data presented below.

2.3 SMS MEASUREMENTS ON A VISCOELASTIC MATERIAL

Figure 2 shows the viscoelastic shear response measured on a freshly prepared PVE sample during a force-distance curve measurement [7]; i.e., during the formation, loading, unloading, and rupture of a contact [24]. The origin for the time axis is taken as the point of maximum applied load (C). The shear modulation amplitude was $X_o \approx$ 0.15 nm. The lower graph displays the force-distance curve. The sample was moved toward the tip at constant speed starting out of contact. Jump-to-contact occurs at point A (t = -36 s). The approach is continued until the predetermined maximum load at C (t = 0 s). Then the direction of motion is reversed until the tip and sample separate at the

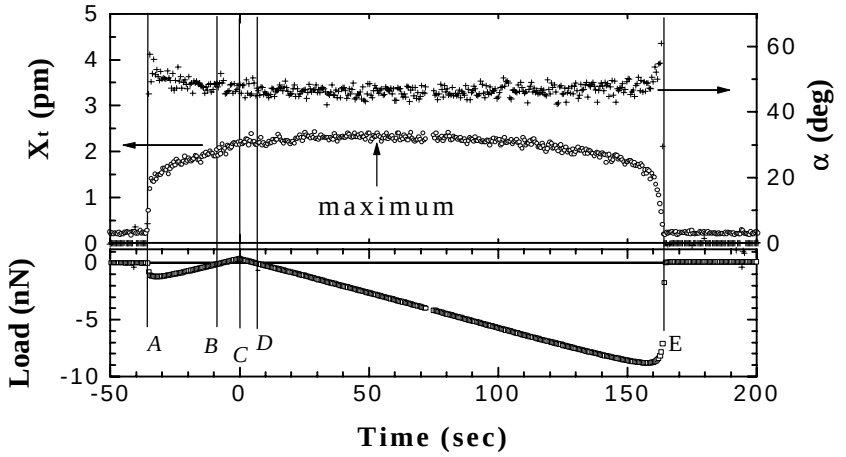

Figure 2. Shear response of a freshly prepared PVE sample during a loading and unloading cycle. The modulation frequency is 1.0 kHz and the modulation amplitude is about 0.13 nm. Lower panel: force-distance curve. Upper panel: amplitude X_t and phase lag α of tip motion on the surface. (From [7].)

pull-off point *E* (t = 164 s). The rounding just prior to pull-off is typical of both macroscopic and scanning force microscope-scale viscoelastic contacts [25,26]. The magnitude of the pull-off force and the degree of rounding depend on the speed, again indicative of the viscoelastic nature of the contact. For times between points *B* and *D*, the contact was under compressive load; otherwise, the load was tensile. The force-distance curve was identical with and without shear modulation indicating that the applied shear modulation does not significantly modify the evolution of the contact.

The upper part of Fig. 2 shows the measured displacement X_t and phase of the scanning force microscope tip. At jump-to-contact (*A*), X_t increases suddenly to about 1.3 pm, then more slowly to about 2.4 pm at maximum load (*C*). X_t continues to increase slightly until $t_{max} \approx 55$ s, long after maximum load was reached, then gradually decreases. Even at its maximum $X_t << X_o$. After the maximum, X_t decreases with the rate of decrease becoming large just as the force-distance curve begins to round significantly prior to pull-off (*E*). Phase response mirrors the amplitude response: increases rapidly to about 60°, then decreases smoothly, reaching a minimum of about 43° at the same time X_t reaches t_{max}. For both amplitude and phase response, the rate of change during jump-to-contact (at *A*) and pull-off (at *E*) is limited by the overall response of the measuring system. The large decrease in phase just after *A* and the increase just prior to *E* may indicate that sliding begins just prior to pull-off.

The maximum value of X_t and the corresponding minimum in phase lag α always occur *after* the contact was under tension (i.e., $F_N < 0$), even for the slowest speeds (50 pm/s). This delayed maximum seems to be a characteristic of viscoelastic materials and was not observed for any of the elastic materials we have also studied; e.g., diamond, mica, silicone [27].

Measurements on PVE were carried out for frequencies over the range 50 Hz $\leq f \leq$ 1.2 kHz and were all qualitatively similar to the results for 1.0 kHz (Fig. 2) except that X_t and varied with frequency as expected for a viscoelastic character of the contact [9].

3 Interpretation of Shear Modulation Spectroscopy Data

This section begins with a discussion of how the contact radius can be determined from the SMS data. The variation of the contact area during loading and unloading is then explained qualitatively in terms of creep using the formalism for contact of viscoelastic bodies developed by Ting [28]. Finally, a more quantitative description that includes interfacial adhesion is evaluated.

3.1 DETERMINATION OF THE CONTACT RADIUS

Perhaps the simplest way to extract information about the materials properties of the contact from the data like that in Fig. 2 is to model the contact using linear springs and dashpots. The simplest mechanical models of this type are the Maxwell and Voigt models [9,29]. We discuss the latter here. In the Voigt model, the viscoelastic component of the contact is described by a linear spring of stiffness $_c$ in parallel with a dashpot with damping coefficient r_c. The cantilever is modeled by a linear spring of stiffness connected in series with the Voigt model. The stiffness of the contact is given in terms of the measurable quantities by

$$_c = \Theta \frac{\left(\frac{X_t}{X_o}\right)\cos - \left(\frac{X_t}{X_o}\right)^2}{1+\left(\frac{X_t}{X_o}\right)^2 - 2\left(\frac{X_t}{X_o}\right)\cos} . \qquad (3)$$

This result was used previously to determine the stiffness of the PVE contact and its increase to the bulk value as the sample aged [7]. The stiffness of the contact is also related to the effective storage shear modulus G^* by [4]

$$_c = 8G^* a . \qquad (4)$$

Since, as already pointed out, $X_t/X_o << 1$, eqns. (3) and (4) can be combined to yield

$$a \cong \left(\frac{\Theta}{8G^*}\right)\left(\frac{X_t}{X_o}\right)\cos \quad . \qquad (5)$$

Assuming constant G^*, eqn. (5) shows that the torsional response of the force sensor is a measure of the contact radius a. This has been pointed out previously for elastic materials [11-13]. This is an important result because the contact radius is one of the most difficult characteristics of a nanometer-scale contact to determine experimentally. Figure 3 is a plot of $(X_t/X_o)\cos\alpha$ calculated from the data in Fig. 2 for times between jump-to-contact and pull-off. The maximum load of 0.4 nN occurs at about 36 s while the maximum in $(X_t/X_o)\cos\alpha$ is at about 85 s. The shaded areas mark regions where the contact may be sliding. The solid curve is a ninth order polynomial fit to the data. Figure 3 shows that the delayed maximum in X_t implies that a reaches its maximum value well after the maximum load has been applied.

3.2 VISCOELACTICITY AND CONTACT AREA

A qualitative understanding of the origin of the delayed maximum in contact area is provided by the work of Ting [28,30]. Following Lee and Radok [31], Ting showed

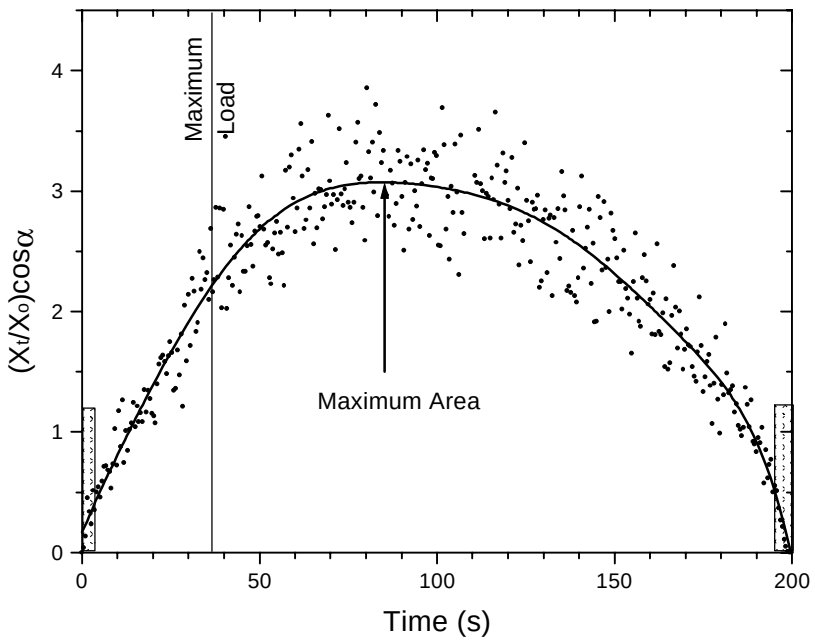

Figure 3. Area function vs. contact time. The maximum load occurs at 36 s and the maximum contact area at about 85 s. The shaded areas indicate time periods where the contact may be sliding.

that the solutions of the Hertzian contact problem can be extended to linear viscoelastic materials if the elastic constants are replaced by corresponding integral operators obtained from the viscoelastic stress-strain relations. For example, if the time evolution of the contact force $F_N(t)$ is known, the contact radius is given by

$$a^3(t) = \frac{3}{8} R \int_0^t \Phi(t - t') \frac{\partial F_n(t')}{\partial t'} dt' \tag{6}$$

where R is the radius of the contacting body and the effective elastic shear modulus G^* has been replaced by an integral operator involving the creep compliance $\Phi(t)$. In contrast to the elastic case, the contact radius now depends on the history of loading through $\partial F_N(t)/\partial t$. As discussed by Ting, care must be taken in determining the upper limit of integration in Eqn. (6) once the area has begun to decrease. Figure 4 gives an example for the case of a rigid spherical indenter on a Maxwell solid. Similar results are obtained for a Voigt model. In this example, the load (Fig. 4a) is a half-sinusoid; $F_N(t) = F_o \sin(t/\ )$ where is the relaxation time of the contact. The contact size (Fig. 4b) continues to grow by creep even after the load has begun to decrease. The time t_{max} at which the maximum contact radius occurs depends on the ratio $t/$ where t is the total contact time. Fig. 4c shows this dependence. The general trend is for t_{max} to occur closer to the time of maximum load as t is increased. As t decreases, t_{max} approaches t. In Fig. 3, the maximum occurs roughly one-third of the way between the time of maximum load and pull-off. From Fig. 4c, we see that this implies that $\approx t$.

The theory of Ting is too simple to provide a quantitative description of Fig. 3. It neglects both adhesion, which is responsible for the pull-off force, and dispersion

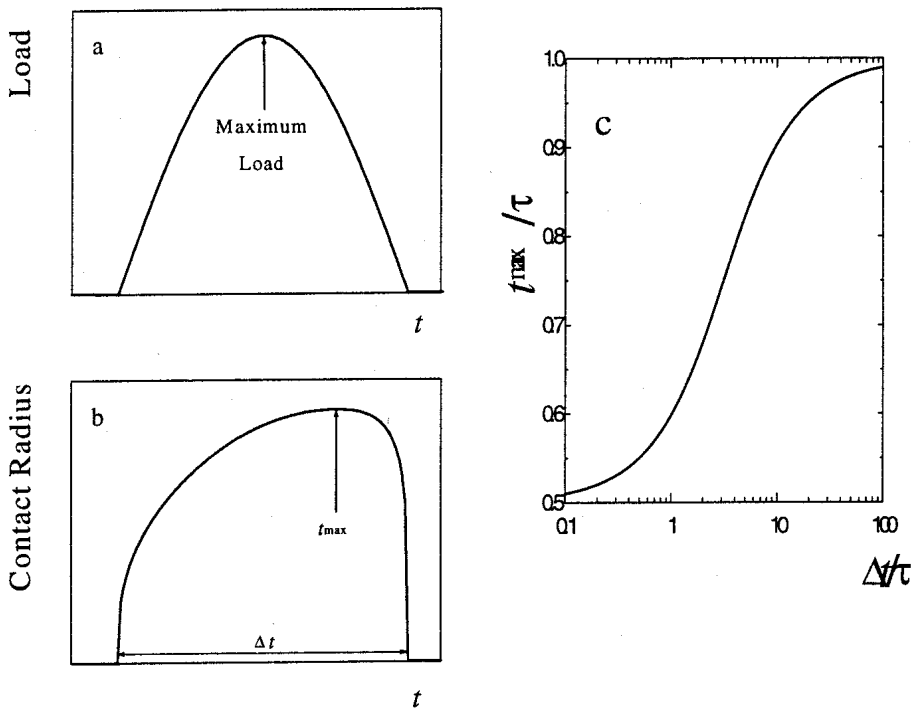

Figure 4. Contact of a rigid sphere with a Maxwell solid. (a) Sinusoidal applied load applied for time Δt. (b) Contact radius a as a function of contact time. (c) t_{max} as a function of the total contact time.

forces, which cause the jump-to-contact. Additionally, freshly prepared PVE is so compliant that, even for the small forces used here, the usual approximation that the diameter of the contact is much smaller than the probe is not satisfied. Appropriate expressions for an elastic indentation by a spherical punch are given by Sneddon [32] and Maugis [33]. We know of no treatment for the case of shear. The contact radius for F_N can be estimated from a Sneddon analysis of the contact and shows that the contact radius at maximum load in Fig. 2 is approximately equal to the nominal tip radius.

Johnson, Kendall and Roberts (JKR) [34] and others [35,36] have shown how adhesion can be incorporated into the theory of elastic contact. Tirrell and co-workers [37] have recently attempted to extend JKR theory to include the effects of linear viscoelasticity. They show that the analog of eqn.(6) is

$$\frac{8}{3R}\int_0^t \Psi(t-t')\frac{\partial a^3}{\partial t'}dt' = F_N(t) + 3\,RW + \sqrt{6\,RWF_N(t) + (3\,RW)^2} \qquad (7)$$

where W is the work of adhesion and $\Psi(t)$ is the stress relaxation function. Equation (7) is only valid as long as the contact radius is increasing; i.e., $t < t_{max}$. Equation (7) was found to give a good description of contacts between 0.7-1.2 mm diameter spheres of diblock copolymers of poly(ethylene)-poly(ethylene-propylene) [37].

We used the data for PVE to evaluate eqn. (7) for the case of nanometer-scale contacts. $F_N(t)$ was taken directly from Fig. 2. The product RW was treated as a parameter for the evaluation of the right hand side (RHS) of eqn. (7). The optimum value ($RW \approx$ 1.85 N) was taken as that which produces a discontinuity in the RHS at the measured

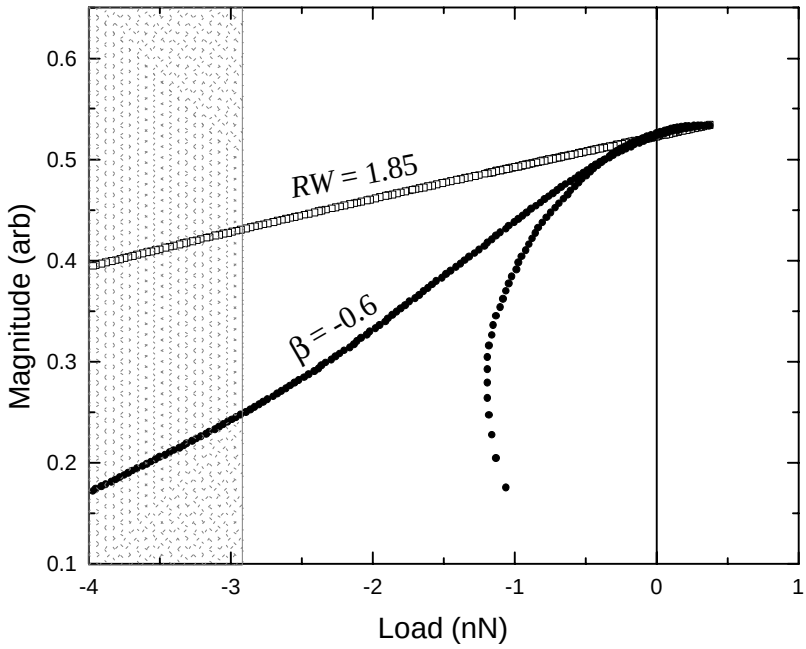

Figure 5. LHS (•'s) and RHS (□'s) of eqn. (7) as a function of the applied load. The shaded region marks the load range for which the contact area is decreasing.

value of the pull-off force. The nominal R of the tips used to obtain the data in Fig. 2 is expected to be in the range 20-50 nm. Thus, $RW \approx 1.85$ nN corresponds to $W \approx$ 40-90 mJ/m^2, which is a reasonable value [5]. The resulting RHS is plotted as the squares in Fig. 5 for the range of $F_N(t)$ for which the contact area (Fig. 3) is increasing.

The left hand side (LHS) of eqn. (7) was evaluated using the ninth order polynomial fit shown in Fig. 2 and assuming that the stress relaxation functions has a power law time dependence of the form

$$\Psi(t) = G_o^* t \tag{8}$$

where G_o^* is zero-frequency value of the effective shear modulus and is the power law exponent. The LHS was evaluated analytically for various values of . The best value of β was taken as that for which the contributions to the LHS for the loading ($t <$ 0 s in Fig. 2) and unloading ($t >$ 0 s) parts of the force-distance curve were identical over the widest range. The resulting LHS is plotted as the dots in Fig. 5 for β = -0.6. The LHS and RHS were normalized at F_N = 0 N by adjusting G_o^*. The resulting $G_o^* \approx$ 2 MPa is consistent with the measured bulk storage modulus assuming a Poisson ratio of 0.5.

It is certainly encouraging that physically reasonable values of the parameters result from applying eqn. (7). However, as can be seen in Fig. 5, the LHS and RHS have significantly different slopes after the maximum load. There is also a large difference in their functional forms during the initial phases of the contact formation. Clearly, the model expressed in eqn. (7) is incomplete. The analysis was also carried out using the stress relaxation functions of the Maxwell and Voigt model but no significant improvement was obtained. What is missing? First, the model assumes that both the interfacial and bulk viscoelasticity properties are identical. Since the polymer molecules

are expected to take up different configurations near the surface [38,39], this may not be a good assumption, particularly since we know that the properties of the PVE samples were continuing to change with sample age [7]. Second, the interfacial adhesion has been assumed to be constant throughout. This will not be true in general, especially when the contact area is changing rapidly. Barquins [25], Barquins and Maugis [40], and Greenwood and Johnson [41] have discussed this from the viewpoint of fracture mechanics but neglected any effects due to creep. These models have also been applied to qualitative interpretation of scanning force microscope force distance curves [26]. Whether or not the conditions required by these theories can be realized experimentally has been questioned [37]. Third, the full range of data in Fig. 3 cannot be analyzed because eqn. (7) does not apply when the contact area is decreasing. Fourth, the analysis given above is only valid if the contact radius a is much smaller than the radius R of the tip. Maugis [33] has shown how to extend JKR theory to this case for elastic, but not viscoelastic, materials. It is not known at present whether all of these effects can be brought together in a single comprehensive theory of viscoelastic contacts with adhesion.

4 Implications for MEMS

The results described in this paper provide a basis for describing the response of MEMS-scale contacts during their formation and separation. The behavior can be complex and rate dependent if adhesion and/or viscoelastic materials, such as lubricants, are involved. For viscoelastic materials, creep can cause the maximum contact area to continue to increase long after the maximum load is reached, even when adhesion is neglected. Adhesion increases the force required to break the contact and, when combined with creep, can substantially increase this pull-off force. The behavior can be complex and is not quantitatively understood at present.

The new technique of Shear Modulation Spectroscopy, described in this paper, offers the possibility to substantially improve our understanding of the mechanics of nanometer-scale contacts.

5 Acknowledgments

The authors thank P. Kleban, R. J. Colton, and K. L. Johnson for useful discussions and encouragement. We are grateful to S. V. Stepnowski for assistance with the measurements, C. M. Roland for providing the PVE samples, and M. Tirrell for providing a preprint prior to publication. The authors thank the Office of Naval Research for support. WNU also acknowledges support from the Department of Energy and the Maine Science and Technology Foundation.

6 References

1. Landman, U., Luedtke, W.D., Burnham, N.A., Colton, R.J. (1990) Atomistic Mechanisms and Dynamics of Adhesion, Nanoindentation, and Fracture, *Science* **248**, 454-461.
2. Johnson, K.L. (1997) Adhesion and friction between a smooth elastic spherical asperity and a plane surface, Proc. Roy. Soc. London A 453, 163-179.

3. Burnham, N.A. and Colton, R.J. (1993) Force Microscopy, in D.A. Bonnell (ed.), *Scanning Tunneling Microscopy and Spectroscopy*, VCH Publishers, New York, pp.191-249.
4. Johnson, K.L. (1985) *Contact Mechanics*, Cambridge University Press, Cambridge.
5. Chaudhury, M.K. (1996) Interfacial interaction between low energy surfaces, *Matl. Sci. Eng. R16*, 97-158.
6. Maboudian, R. and Howe, R. T. (1997) Critical Review: Adhesion in surface micromechanical structures, *J. Vac. Sci. Technol. B* **15**, 1-20.
7. Wahl, K.J., Stepnowski, S.V. and Unertl, W.N. (1997) Viscoelastic effects in nanometer-scale contacts under shear, *Tribology Lett*. (submitted).
8. Bhushan, B., Israelachvili, J.N., and Landman, U. (1995) Nanotribology: friction, wear and lubrication at the atomic scale, Nature 374, 607-616.
9. Ferry, J.D. (1980) *Viscoelastic Properties of Polymers*, John Wiley, New York.
10. Yamanaka, K. and Tomita, E. (1995) Lateral Force Modulation Atomic Force Microscope for Selective Imaging of Friction Forces, *Jpn. J. Appl. Phys*. **34**, 2879-2882.
11. Carpick, R.W., Ogletree, D. F. and Salmeron, M. (1997) Lateral stiffness: a new nanomechanical measurement for the determination of shear strengths with friction force microscopy, *Appl. Phys. Lett.* **70**, 1548-1550.
12. Lantz, M.A., O'Shea, A. C., Hoole, F. and Welland, M.E. (1997) Lateral stiffness of the tip and tip-sample contact in frictional force microscopy, *Appl. Phys. Lett*. **70**, 970-972.
13. Lantz, M.A., O'Shea, A. C., Welland, M.E. and K. L. Johnson (1997) Atomic-force-microscope study of contact area and friction on $NbSe_2$, *Phys. Rev. B* **55**, 10776-10785.
14. Luengo, G., Schmitt, F.J., Hill, R., and Israelachvili, J. (1997) Thin film Rheology and Tribology of Confined Polymer Melts: Contrasts with Bulk Properties, *Macromolecules* **30**, 2482-2494.
15. Granick, S. and Hu, H.W. (1994) Nanorheology of Confined Polymer Melts. 1. Linear Shear Response at strongly Adsorbing surfaces, *Langmuir* **10**, 3857-3866.
16. Georges, J. M., Tonck, A., Loubet, J.L., Mazuyer, D., Georges, E. and Sidoroff, F. (1996) Rheology and Friction of Compressed Polymer Layers Adsorbed on Solid surfaces, *J. Phys. II France* **6**, 57-76.
17. Cohen, S.R., Neubauer, G., and McClelland, GM, Nanomechanics of a Au-Ir contact using a bidirectional atomic force microscope, *J. Vac. Sci. Technol. A* **8** (1990) 3449.
18. Burnham, N.A., Gremaud, G., Kulik, A.J., Gallo, P.J., and Oulevey, F. (1996) Materials' properties measurements: Choosing the optimum scanning probe microscope configuration, *J. Vac. Sci. Technol. B* **14**, 1308-1312.
19. Tanaka, K., Taura, A., Ge, S.R., Takahara, A., and Kajiyama, T. (1996) Molecular Weight Dependence of Surface Dynamic Viscoelastic Properties for the Monodisperse Polystyrene Film, *Macromolecules* **29**, 3040-3042.
20. Mazeran, P.E. and Loubet, J.L. (1997) Force modulation with a scanning force microscope: an analysis, *Tribology Lett.* **3**, 125-132.
21. Koleske, D.D., Lee, G.U, Gans, B.I., Lee, K.P., DiLella, D.P., Wahl, K.J., Barger, W.R., Whitman, L.J. and Colton, R.J. (1995) ,Design and calibration of a scanning force microscope for friction, adhesion, and contact potential studies, *Rev. Sci. Instrum.* **66** 4566-4574.
22. Ogletree, D.f., Carpick, R.W. and Salmeron, M. Calibration of frictional forces in atomic force microscopy, *Rev. Sci. Instrum.* **67**, 3298-3306.

23. Roland, C. M. (1994) Constraints on Local Segmental Motion in Poly(vinylethylene) Networks, *Macromolecules* **27**, 4242-4247.
24. Burnham, N.A., Colton, R.J., and Pollock, H.M. (1993) Interpretation of force curves in force microscopy, *Nanotechnology* **4**, 64-80.
25. Barquins, M. (1982) Influence of Dwell Time on the Adherence of Elastomers, *J. Adhesion* **14**, 63-82.
26. Aimé, J.P., Elkaakour, Z., Odin, C., Bouhacina, T., Michel, T., Curély, J. and Dautant, A. (1994) Comments on the use of the force mode in atomic force microscopy for polymer films, *J. Appl. Phys*. 76, 754-762.
27. K. J. Wahl, S. V. Stepnowski and W. N. Unertl (to be published).
28. Ting, T. C. T. (1966) The Contact Stresses Between a Rigid Indenter and a Viscoelastic Half-Space, *J. Appl. Mech*. **33**, 845-854.
29. Harris, C.M. (ed) (1996) *Shock and Vibration Handbook*, 4th edition, McGraw-Hill, New York, p. 2.5.
30. Ting, T.C.T. (1968) Contact Problems in the Linear Theory of Viscoelasticity, *J. Appl. Mech*. **35**, 248-254.
31. Lee, E.H. and Radok, J.R.M. (1960) The Contact Problem for Viscoelastic Bodies, *J. Appl. Mech*. **27**, 438-444.
32. Sneddon, J. N. (1965) *Int. J. Eng*. **3**, 47.
33. Maugis, D. (1995) Extension of the Johnson-Kendall-Roberts Theory of the Elastic Contact of Spheres to Large Contact Radii, *Langmuir* **11**, 679-682.
34. Johnson, K.L., Kendall, K. and Roberts, A.D. (1971) Surface energy and the contact of elastic solids, *Proc. R. Soc. London A* **324**, 301-313.
35. Derjaguin, B.V., Muller, V.M. and Toporov, Y.P. (1975) Effect of Contact Deformations on the Adhesion of Particles, *J. Colloid Interface Sci*. **53**, 314-326.
36. Greenwood, J. A. (1997) Adhesion of Elastic Spheres, *Proc. R. Soc. London* **A** 453, 1277-1297.
37. Falsafi, A., Deprez, P., Bates, F. S. and Tirrell, M. (1997) Direct Measurement of adhesion between viscoelastic polymers: A contact mechanical approach, *J. Rheology* (submitted).
38. Tanaka, K., Takahara, A., and Kajiyama, T. (1995) Surface molecular motion in thin films of poly(styrene-block-methyl methacrylate) diblock copolymer, *Acta Polymer* **46**, 476-482.
39. Mayes, A.M. (1994) Glass Transition of Amorphous Polymer Surfaces, *Macromolecules* **27**, 3114-3115.
40. Barquins, M. and Maugis, D. (1981) Tackiness of Elastomers, *J. Adhesion* **13**, 53-65.
41. Greenwood, J.A. and Johnson, K.L. (1981) The mechanics of adhesion of viscous solids, *Phil Mag. A* **43**, 697-711.